Journal of Power Sources 222 (2013) 288–293

Contents lists available at SciVerse ScienceDirect

Journal of Power Sources

journal homepage: www.elsevier.com/locate/jpowsour

Assessment of $LnBaCo_{1.6}Ni_{0.4}O_{5+\delta}$ (Ln = Pr, Nd, and Sm) double-perovskites as cathodes for intermediate-temperature solid-oxide fuel cells

Xiangli Che, Yu Shen, Hang Li, Tianmin He*

Key Laboratory of Physics and Technology for Advanced Batteries, Ministry of Education, College of Physics, Jilin University, 2699 Qianjin Street, Changchun, 130012, PR China

HIGHLIGHTS

- Investigation on structure and properties of double-proveskites $LnBaCo_{1.6}Ni_{0.4}O_{5+\delta}$ as IT-SOFC cathodes.
- Thermal expansion coefficients of $LnBaCo_{1.6}Ni_{0.4}O_{5+\delta}$ are lowered while retaining desirable electrochemical performance.
- $LnBaCo_{1.6}Ni_{0.4}O_{5+\delta}$ exhibits good chemical compatibility with SDC electrolyte at temperatures below 950 °C.

ARTICLE INFO

Article history:
Received 4 June 2012
Received in revised form
14 August 2012
Accepted 16 August 2012
Available online 7 September 2012

Keywords:
Solid-oxide fuel cell
Double-perovskite
Cathode
Electrical conductivity
Thermal expansion
Electrochemical performance

ABSTRACT

Nickel-substituted double-perovskites, $LnBaCo_{1.6}Ni_{0.4}O_{5+\delta}$ (LnBCN, Ln = Pr, Nd and Sm), are investigated as potential cathode materials for intermediate-temperature solid-oxide fuel cells based on the $Ce_{0.8}Sm_{0.2}O_{1.9}$ (SDC) electrolyte. The LnBCN materials exhibit high chemical compatibility with the SDC electrolyte at 950 °C for 2 h. Substitution of Ni for Co decreases the thermal expansion coefficient and the electrical conductivity, as compared with the nickel-free samples while retaining desirable electrochemical performance. The area-specific resistances of the LnBCN samples on the SDC electrolyte where Ln = Pr, Nd, and Sm at 700 °C are 0.056, 0.077, and 0.11 $\Omega\,cm^2$, respectively. For Ln = Pr, Nd, and Sm cathodes, the maximum power densities of the electrolyte-supported Ni-SDC/SDC/LnBCN single cells with a 0.3 mm thick SDC electrolyte reach 732, 714, and 572 $mW\,cm^{-2}$ at 800 °C, respectively. These results show that nickel-substituted LnBCN double-perovskites are potential cathode candidates for use in IT-SOFCs.

1. Introduction

Solid-oxide fuel cells (SOFCs) are all-solid electrochemical energy conversion devices that directly convert the chemical energy in fuel to electricity with high conversion efficiency and low pollution emission. One of the major challenges in the development of SOFCs is the reduction of their operating temperature to the intermediate-temperature (IT) range of 600–800 °C in order to improve the reliability and lifetime of the cell system and to lower the costs [1]. However, with the reduction of the operating temperature, the cathodic polarization resistances sharply increase because the kinetics of the oxygen reduction reaction is considerably slower at temperatures below 800 °C [2]. Therefore, the development of new cathode materials with high electrocatalytical activity in the intermediate-temperature range is vital to achieving the goals of IT-SOFC technologies [3].

One strategy for developing IT-SOFC cathodes is to use a mixed electronic and ionic conductor (MIEC), such as Sr-doped $LnCoO_3$ (Ln: lanthanide) and their derivatives, to replace the conventional Sr-doped $LaMnO_3$ cathode [4,5]. By introducing bulk ion transport, the oxygen species may be transported through the bulk of the electrode, and the electrochemically active region can be extended to a finite width from the electrode/electrolyte interface, thereby improving the kinetics at temperatures below 800 °C [2,4,6,7]. The $LnBaCo_2O_{5+\delta}$ (Ln = La, Pr, Nd, Sm, Gd, and Y) double-perovskites were recently developed as potential cathode materials for IT-SOFCs because of their high electronic conductivity and sufficient oxygen ionic transport [8–17]. For example, $LnBaCo_2O_{5+\delta}$ (Ln = Pr, Nd, Sm, and Gd) materials show >340 $S\,cm^{-1}$ conductivity at 800 °C [18], which meets the electrical conductivity requirement of IT-SOFC cathode materials. The oxygen ionic conductivity of the $GdBaCo_2O_{5+\delta}$ sample was reported to be 0.01 $S\,cm^{-1}$ at 500 °C [19]. The bulk diffusion in $PrBaCo_2O_{5+\delta}$ is larger than that in

* Corresponding author. Tel./fax: +86 431 85166112.
E-mail addresses: hly@mail.jlu.edu.cn, hetm@jlu.edu.cn (T. He).

0378-7753/$ – see front matter © 2012 Elsevier B.V. All rights reserved.
http://dx.doi.org/10.1016/j.jpowsour.2012.08.044

$GdBaCo_2O_{5+\delta}$ [13], implying that the former has a higher ionic conductivity than the latter under the same conditions. The attractive MIEC properties of $LnBaCo_2O_{5+\delta}$ make this system more suitable for use as an IT-SOFC cathode. However, like other Co-containing perovskite cathodes, the high thermal expansion coefficient (TEC) of $LnBaCo_2O_{5+\delta}$ is a major factor in the development of double-perovskite cathodes. For Co-based perovskite cathodes, a thermally induced spin-state transition of the Co^{3+} ion from the low spin (or intermediate spin) to the high-spin states is responsible for the high TECs [20–22]. Thus, the lowering of the Co content in Co-containing cathodes is one of the more effective approaches for TEC reduction. Kim et al. [22] and Wei et al. [23] separately demonstrated that the substitution of a small amount of Co with Ni in $NdBaCo_2O_{5+\delta}$ and $GdBaCo_2O_{5+\delta}$ can effectively reduce the TECs of these materials. For example, the TEC of $GdBaCo_{2-x}Ni_xO_{5+\delta}$ materials between 30 and 900 °C decreased from $20.0 \times 10^{-6}\ K^{-1}$ for $x = 0.0$–$15.5 \times 10^{-6}\ K^{-1}$ for $x = 0.3$ [23].

To lower TECs while maintaining high cathode performance, $LnBaCo_{1.6}Ni_{0.4}O_{5+\delta}$ (LnBCN, Ln = Pr, Nd, and Sm) double-perovskites are systematically investigated as a potential cathode material for IT-SOFCs. The TECs of the LnBCNs can be lowered to maximize the substitution of Co by Ni to take into account the solid solubility limit of Ni in the LnBCNs [24]. Thus, 20% Co ions were substituted with Ni. The phase composition, chemical compatibility, electrical conductivity, TEC, and electrochemical performance of the LnBCN materials are presented.

2. Experimental

The double-perovskite $LnBaCo_{1.6}Ni_{0.4}O_{5+\delta}$ (LnBCN, Ln = Pr, Nd, and Sm) samples were synthesized via a modified sol-gel process. Citrate and ethylenediamine tetraacetic acid (EDTA) were used as parallel complexing agents. Pr_6O_{11} (99.9%), Nd_2O_3 (99.9%), Sm_2O_3 (99.9%), $Ba(NO_3)_2$ (99%), $Co(NO_3)_2 \cdot 6H_2O$ (99%), and $Ni(NO_3)_2 \cdot 6H_2O$ (99.9%) were used as the starting materials. The required amounts of the above chemicals were prepared into their respective mixed solutions according to the molecular composition of LnBCN. EDTA and citric acid were introduced at a molar ratio of EDTA:citric acid:total metal ions at 1:1.5:1. The pH of the solution was adjusted to 8 by adding a $NH_3 \cdot H_2O$ solution. After converting the sample into a viscous gel under heating and stirring conditions, the viscous gel was dried at 150 °C for 10 h to form a powder precursor. The precursor powders were first calcined at 1000 °C for 10 h. The LnBCN powders were then pressed into pellets (13 mm in diameter and 1 mm thickness) and cylinders (6 mm in diameter, 5–6 mm thickness) at 200 MPa and subsequently sintered at 1200 °C for 10 h. $Ce_{0.8}Sm_{0.2}O_{1.9}$ (SDC) and NiO powders were synthesized via the glycine-nitrate process. Dense SDC samples were prepared by pressing the powders into pellets (13 mm in diameter) and sintering at 1400 °C for 10 h in air. The thickness of the final SDC pellets was fixed at 0.3 mm by grinding the two sides of the samples. The composite anode was prepared by mixing NiO powders with SDC powders at a weight ratio of 65:35.

Phase purity and structural analyses were performed using an X-ray diffractometer (Rigaku-D-Max γA, $\lambda = 0.15418$ nm) at an angle of 0.02° and in the 20–80° scanning range. The chemical compatibilities of the LnBCN samples with the SDC electrolyte were investigated by calcining a mixture of the two material powders in air at 950 °C for 2 h.

The electrical conductivities of the samples sintered at 1200 °C for 10 h were measured in air using the van der Pauw method from 300 °C to 850 °C. The TEC of the samples sintered at 1200 °C for 10 h was measured in air using a dilatometer (Netzsch DIL 402C) in the 30 °C to 1000 °C temperature range. A heating rate of 5 °C min^{-1} and an air flow rate of 60 mL min^{-1} were used. Symmetrical LnBCN/SDC/LnBCN cells were prepared by screen-printing and calcining at 950 °C for 2 h in air. The symmetrical cells were then analyzed via impedance spectroscopy using an electrochemical analyzer (CHI 604D, Chenhua, China). Measurements were performed in the 0.1 Hz to 100 kHz frequency range and at an AC amplitude of 10 mV under open-circuit conditions. The impedance data were fitted using Z-View 3.1 software. Electrolyte-supported Ni-SDC/SDC/LnBCN single cells were prepared via screen-printing. The anode layer on the SDC electrolyte was first sintered at 1250 °C for 4 h. The cathode layer on the opposite side of the SDC was subsequently fired at 950 °C for 2 h. The single cells were examined from 600 °C to 800 °C, with dry hydrogen as the fuel and ambient air as the oxidant. The fuel flow rate was approximately 100 mL min^{-1}.

3. Results and discussion

3.1. XRD analysis, crystal structure, and chemical compatibility

Fig. 1(a)–(c) show the XRD patterns of the LnBCN (Ln = Pr, Nd, and Sm) samples after sintering at 1200 °C for 10 h in air. The XRD patterns clearly indicate that all LnBCN samples formed double-perovskite structures. No appreciable impurity peaks were observed for these Ni-substituted samples. All samples are single-phase, indicating that, first, the phase-pure LnBCN samples can be obtained by sintering at 1200 °C for 10 h and, second, that the Ni content is lower than the solid solubility limit of Ni in LnBCN [22,24]. The XRD patterns of the PrBCN and NdBCN samples in Fig. 1(a) and (b) can be indexed as primitive tetragonal structures with the *P4/mmm* space group, which is in agreement with $NdBaCo_{2-x}Ni_xO_{5+\delta}$ ($0 \le x \le 0.4$) data reported by Kim et al. [22]. The XRD pattern of the SmBCN sample in Fig. 1(c) is indexed to the primitive orthorhombic structure with *Pmmm* symmetry, which is consistent with the $GdBaCo_{2-x}Ni_xO_{5+\delta}$ ($0 \le x \le 0.4$) crystal structures reported by Wei et al. [23] and Bharathi et al. [24].

The crystal structure of $LnBaCo_2O_{5+\delta}$ is closely associated with the lanthanide ionic radius and the oxygen content [25–27]. An earlier study showed that $LnBaCo_2O_{5+\delta}$ oxides with a larger lanthanide ionic radius (such as Pr^{3+} and Nd^{3+}) can be crystallized into a tetragonal structure, whereas those with an intermediate

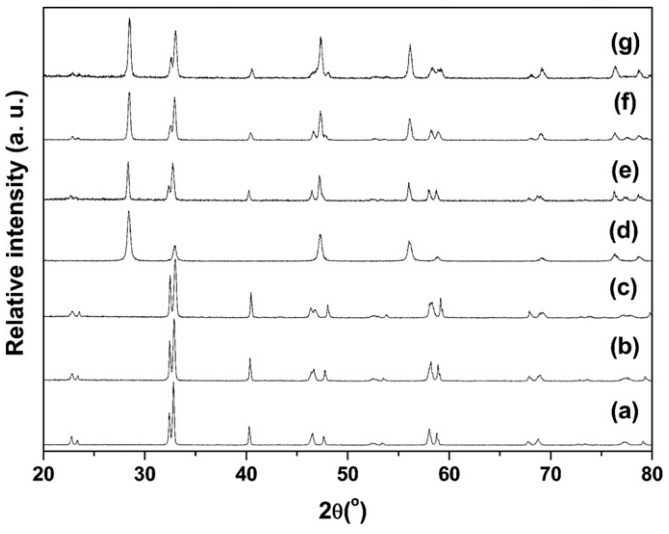

Fig. 1. XRD patterns of the LnBCN samples and LnBCN–SDC mixtures: (a) PrBCN, (b) NdBCN, (c) SmBCN, (d) SDC, (e) PrBCN-SDC, (f) NdBCN-SDC, and (g) SmBCN-SDC. The LnBCN and SDC samples were sintered in air at 1200 and 1400 °C for 10 h, respectively. The LnBCN–SDC mixtures were calcined at 950 °C for 2 h.

lanthanide ionic radius (such as Sm^{3+} and Gd^{3+}) can be crystallized into an orthorhombic structure [25,26]. Therefore, all XRD patterns of the PrBCN and NdBCN samples can be indexed to a tetragonal structure, whereas that of the SmBCN sample is indexed to an orthorhombic structure. Kim et al. [22] studied the crystal structure of $NdBaCo_{2-x}Ni_xO_{5+\delta}$ ($0 \le x \le 0.6$) materials. They found that the $x = 0.6$ sample exhibited peak broadening at $2\theta \approx 46.5^\circ$ and 77.5°, which is a key structural characteristic of the orthorhombic phase in such materials. Fig. 2 shows the magnified XRD patterns of the LnBCN samples in the $45^\circ \le 2\theta \le 80^\circ$ range. The XRD patterns of the PrBCN and NdBCN samples are highly different from that of the SmBCN sample at $2\theta \approx 46$–47° and 76.5–78.5°. Broadened XRD peaks are clearly observed in the SmBCN sample, suggesting that SmBCN crystallizes into an orthorhombic structure. The unit-cell parameters of the LnBCN samples are listed in Table 1. The unit-cell parameters of NdBCN are in agreement with the data reported by Kim et al. [22].

Fig. 1(e)–(g) show the XRD patterns of the LnBCN and SDC mixtures after calcining at 950 °C for 2 h in air. All XRD peaks can be indexed to a physical mixture of the LnBCN and SDC phases. No additional diffraction peaks nor distinct shifts in the diffraction peaks are observed, suggesting that the LnBCN materials are chemically compatible with the SDC electrolyte at 950 °C for 2 h. Kim et al. [22] also demonstrated that the $NdBaCo_{2-x}Ni_xO_{5+\delta}$ and $Gd_{0.2}Ce_{0.8}O_{1.9}$ (GDC) mixture was chemically compatible when $x = 0.0$, 0.4, and 0.6 after calcining at 1000 °C for 3 h, which provides good support for the chemical compatibility in this work.

3.2. Thermal expansion and electrical behaviors

Fig. 3 shows the thermal expansion curves of the LnBCN samples at temperatures between 30 and 1000 °C in air. The average TECs are listed in Table 1. The TECs of the samples significantly decrease with the change from Ln = Pr to Sm. This decrease is mainly due to the decrease in the ionicity of the Ln–O bonds because of the generally larger thermal expansion of ionic bonds compared with that of covalent bonds [12]. Compared with undoped $LnBaCo_2O_{5+\delta}$ cathodes, the substitution of Ni for Co lowers the TECs of the LnBCN samples in the 30–1000 °C temperature range in air, from $21.5 \times 10^{-6}\ K^{-1}$ for $PrBaCo_2O_{5+\delta}$ to $20.6 \times 10^{-6}\ K^{-1}$ for PrBCN, from $21.0 \times 10^{-6}\ K^{-1}$ for $NdBaCo_2O_{5+\delta}$ to $19.4 \times 10^{-6}\ K^{-1}$ for NdBCN, and from $19.1 \times 10^{-6}\ K^{-1}$ for $SmBaCo_2O_{5+\delta}$ to $16.6 \times 10^{-6}\ K^{-1}$ for SmBCN. These values are ~4%, 8%, and 13% lower than those of the $LnBaCo_2O_{5+\delta}$ for Ln = Pr, Nd, and Sm, respectively. The TEC of NdBCN in this study is higher than that reported by Kim et al. ($16.9 \times 10^{-6}\ K^{-1}$ in the 80 °C to 900 °C temperature range) [22]. Attempts to reduce the TEC further are hindered because of the lower solid solubility limit of the Ni in the LnBCN. The reduction in the TEC of the LnBCN samples can be attributed to the decrease in the Co content. As mentioned in the Section 1, the spin state transition of the Co^{3+} ion from the low-spin to the high-spin states is responsible for the high TECs [20–22]. The substitution of Ni for Co in $LnBaCo_2O_{5+\delta}$ decreases the Co content, which results in the decrease in the spin-state transition of the Co^{3+} ions and lowers the TECs of LnBCN compared with those of the undoped $LnBaCo_2O_{5+\delta}$.

Table 1
Unit-cell parameters and thermal expansion coefficients (TECs) of the LnBCN (Ln = Pr, Nd, and Sm) materials.

Samples	Unit-cell parameters				TEC × 10^{-6} (K^{-1})
	a (nm)	*b* (nm)	*c* (nm)	*V* (nm^3)	
PrBCN	0.39076		0.76375	0.11662	20.6
NdBCN	0.39022		0.76200	0.11603	19.4
SmBCN	0.39162	0.38874	0.75769	0.11608	16.6

Fig. 4 shows the variations in the electrical conductivity of the LnBCN (Ln = Pr, Nd, and Sm) samples with temperature. The electrical conductivities of the LnBCN samples decrease with increasing temperature, which is indicative of a metallic conducting behavior. At a given temperature, the electrical conductivity of the LnBCN samples decreases from Ln = Pr to Sm because of the increase in the oxygen vacancy concentration, as well as the consequent perturbation of the O–Co–O interaction and carrier delocalization [12].

The electrical conductivities of the LnBCN samples decrease compared with those of the undoped $LnBaCo_2O_{5+\delta}$ cathodes [18]. This result is mainly due to the increase in the oxygen vacancy concentration in LnBCN, which results in a decrease in the carrier concentration. Kim et al. [22] demonstrated that the oxygen content in $NdBaCo_2O_{5+\delta}$ decreases with increasing Ni content. For example, the oxygen content in $NdBaCo_2O_{5+\delta}$ decreased from 5.85 for the $x = 0.0$ sample to 5.78 for the $x = 0.4$ sample with increasing Ni content. Electron transport in $LnBaCo_2O_{5+\delta}$ may be achieved by the electron transfer between multivalent metal ions at the B-site and oxygen ion [12] via the adjacent Co^{3+}–O–Co^{4+} connecting network. The Co ion concentration in LnBCN materials is decreased

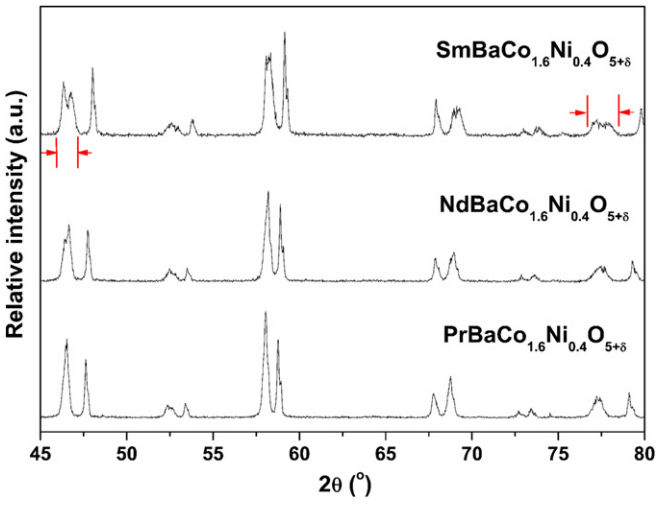

Fig. 2. Magnified XRD patterns of the LnBCN samples (Ln = Pr, Nd, and Sm).

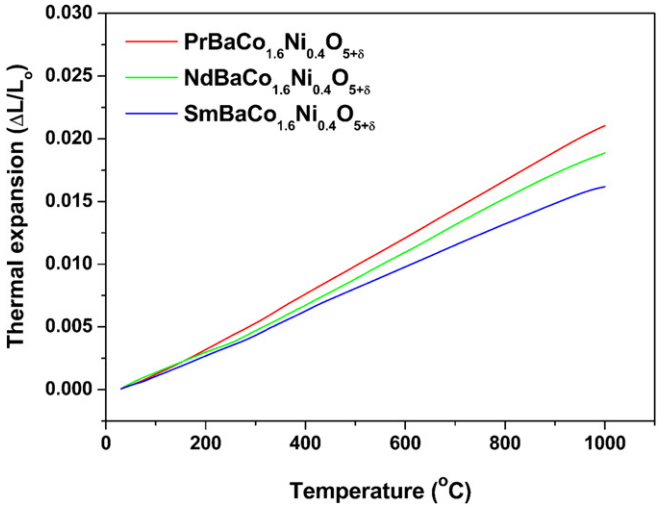

Fig. 3. Thermal expansion curves of the LnBCN samples (Ln = Pr, Nd, and Sm) between 30 and 1000 °C in air.

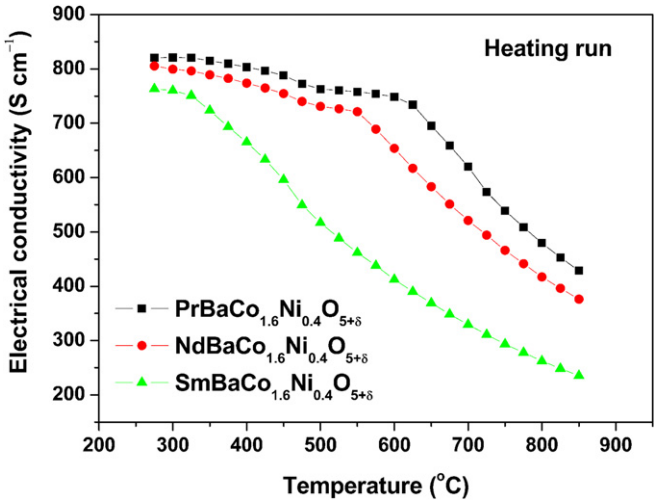

Fig. 4. Temperature dependence of the electrical conductivity of the LnBCN samples (Ln = Pr, Nd, and Sm) in air.

because of the substitution of Ni for Co. In addition, the electron transport is further hindered, thus resulting in a decreased electrical conductivity. The electrical conductivity of the LnBCN samples is higher than 235 S cm^{-1} at temperatures between 300 and 850 °C in air, which meets the electrical property requirements of IT-SOFC cathodes.

3.3. Impedance spectroscopy

Fig. 5 shows the typical impedance spectra of the LnBCN/SDC/LnBCN symmetrical cells measured in air at 600 and 800 °C. The ohmic resistance was deducted to facilitate the comparison. The impedance spectra consist of a high-frequency arc and a low-frequency arc, which indicate the occurrence of at least two electrode oxygen reduction processes. The electrode process at the high-frequency arc corresponds to the oxygen ion-transfer process at the interface of the LnBCN electrode and the SDC electrolyte. The electrode processes at the low-frequency arc are a combination of the dissociation and surface diffusion of oxygen species [28]. The resistance between the two intercepts at the real axis is established as the area-specific resistance (ASR) of the two interfaces. The total ASRs are divided by two to obtain the single ASR. The fitted data of the impedance spectra at different temperatures are listed in Table 2. The equivalent circuit is shown in the inset of Fig. 5. Fig. 5 and Table 2 show that the ASRs increase with the change from Ln = Pr to Sm primarily due to the decrease in electrical conductivity of the samples. For example, the conductivities of the Ln = Pr, Nd, and Sm samples range from 749 cm^{-1} to 479 cm^{-1}, from 654 cm^{-1} to 417 cm^{-1}, and from 412 cm^{-1} to 262 S cm^{-1} in the 600 °C to 800 °C temperature range, respectively.

The ASRs of the LnBCN cathodes on the SDC electrolyte are 0.056, 0.077, and 0.11 Ω cm^2 at 700 °C for Ln = Pr, Nd, and Sm, respectively. For a cathode material, the generally accepted target ASR at the operating temperature is below 0.15 Ω cm^2 [29]. In this study, all of the ASRs of the LnBCN cathodes on the SDC electrolytes are below 0.15 Ω cm^2 at 700 °C, which meets the ASR requirement for cathodes. Zhao et al. [30], Chen et al. [31], and Zhu et al. [32] reported that the ASRs of $PrBaCo_2O_{5+\delta}$ cathodes on SDC electrolytes are 0.078, 0.07959, and 0.259 Ω cm^2 at 700 °C, respectively. Zhou et al. [14] reported that the ASR of the $SmBaCo_2O_{5+\delta}$ cathode on the SDC electrolyte is 0.19 Ω cm^2 at 700 °C. Zhang et al. [13] reported that the $PrBaCo_2O_{5+\delta}$ cathode ASR on the SDC

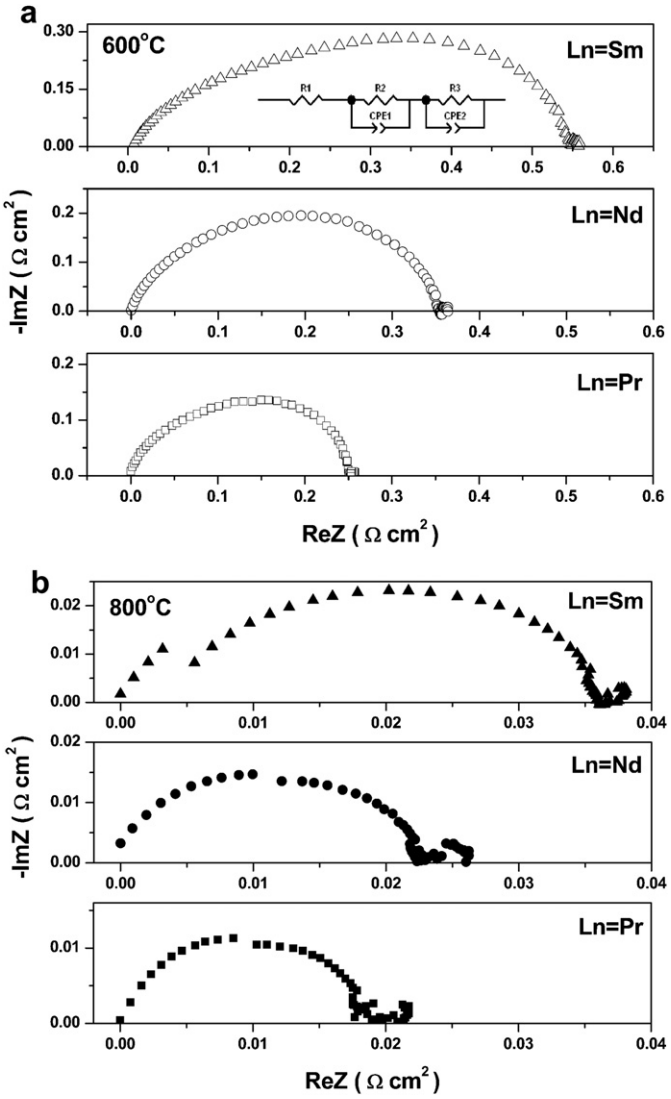

Fig. 5. Typical impedance spectra of the LnBCN/SDC/LnBCN (Ln = Pr, Nd, and Sm) symmetrical cells at 600 and 800 °C in air. The ohmic resistance was subtracted from the experimental data.

electrolyte is 0.213 Ω cm^2 at 600 °C. Compared with the ASRs of the $LnBaCo_2O_{5+\delta}$ cathodes on LSGM electrolytes, those of the $LnBaCo_2O_{5+\delta}$ cathodes on the same electrolytes are 0.070, 0.093, and 0.110 Ω cm^2 at 700 °C, respectively, with the change from Ln = Pr to Sm [18]. Peña-Martínez et al. [33] showed that the ASRs of the $GdBaCo_2O_{5+\delta}$ cathode on the LSGM electrolyte are ~0.41, 0.23, and 0.14 Ω cm^2 at 700, 750, and 800 °C, respectively. Comparison shows that the partial substitution of Ni for Co decreases the ASRs of the LnBCN cathodes on the SDC electrolytes.

Table 2
Area-specific resistances (ASRs) of LnBCN (Ln = Pr, Nd, and Sm) cathodes on $Ce_{0.8}Sm_{0.2}O_{1.9}$ (SDC) electrolytes.

Temperature	PrBCN on SDC (Ω cm^2)	NdBCN on SDC (Ω cm^2)	SmBCN on SDC (Ω cm^2)
600 °C	0.25	0.35	0.55
650 °C	0.11	0.16	0.24
700 °C	0.056	0.077	0.11
750 °C	0.029	0.037	0.058
800 °C	0.018	0.023	0.036

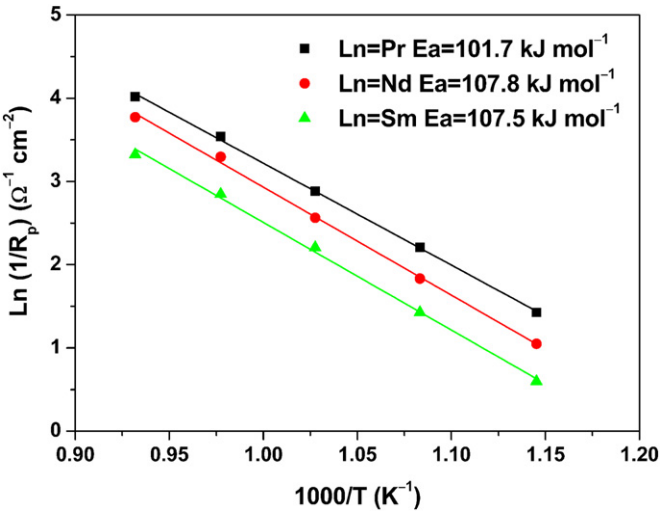

Fig. 6. Arrhenius plots of the ASRs for the LnBCN samples (Ln = Pr, Nd, and Sm).

This result indicates that the LnBCN materials display high catalytic activity for use as IT-SOFC cathodes. The enhanced cathode performance can be attributed to the decrease in the TECs of the LnBCN samples. In addition, Kim et al. [22] reported that the oxygen vacancies in $NdBaCo_{2-x}Ni_xO_{5+\delta}$ cathodes increase with increasing Ni substitution. Therefore, the increase in the oxygen vacancy concentration is another reason for the improvement in the LnBCN cathode performance. In addition, the results obtained in this study are also significantly lower than those of the Ni-containing simple-perovskite cathodes. For example, the ASR of the $La_{0.6}Sr_{0.4}Ni_{0.2}Fe_{0.8}O_{3-\delta}$ cathode on the SDC electrolyte is 0.5 Ω cm^2 at 700 °C [34]; those of the $LaNi_{0.6}Fe_{0.4}O_3$ cathode on the SDC electrolyte are 1.3 Ω cm^2 at 800 °C [35] and 2.4 Ω cm^2 at 700 °C [36], respectively; and that of the $La_{0.6}Ca_{0.4}Fe_{0.8}Ni_{0.2}O_3$ cathode on the SDC electrolyte is 0.44 Ω cm^2 at 850 °C [37].

Fig. 6 shows the Arrhenius plots of the ASRs of the LnBCN cathodes on the SDC electrolytes. The activation energies, which were calculated from the slopes of the Arrhenius plots, are 101.7, 107.8, and 107.5 kJ mol^{-1}. These results are lower than those for the $SmBaCo_2O_{5+\delta}$ cathode on the SDC electrolyte within the same temperature range [14]. The activation energies of the LnBCN cathodes are also lower than those of the Ni-containing simple-perovskite cathodes. For example, the activation energy of the $La_{0.6}Sr_{0.4}Ni_{0.2}Fe_{0.8}O_{3-\delta}$ cathode is 127.5 kJ mol^{-1} [34] while that of the $LaNi_{0.6}Fe_{0.4}O_3$ cathode is 133 kJ mol^{-1} [35], both on SDC electrolytes. These results confirm that the LnBCN cathodes exhibit high catalytic activities for oxygen reduction reactions.

3.4. Single-cell performance

Fig. 7 shows the *I–V* and *I–P* curves of the Ni-SDC/SDC/LnBCN cells, which were measured at different temperatures using dry H_2 as the fuel and ambient air as the oxidant. The open-circuit voltages (OCVs) of the cells are all below 1.0 V. The low OCVs are due to the partial reduction of Ce^{4+} to Ce^{3+} in the SDC electrolyte under a reducing atmosphere, which results in electronic conductivity and internal short-circuits [38]. The low OCVs of the cells can be improved by using oxygen-ion-conducting electrolytes (e.g., doped $LaGaO_3$) or proton-conducting electrolytes (e.g., doped $BaCeO_3$ [39]) instead of an SDC electrolyte. The cell performance of the LnBCN cathodes decreases with the shift from Ln = Pr to Sm because of the decreasing electrical conductivity and increasing ASR. At 800 °C, the maximum power densities of the cells in the Ln = Pr, Nd, and Sm cathodes are 732, 714, and 572 mW cm^{-2}, respectively. Kim et al. [22] also showed that the cell performances of the $NdBaCo_{2-x}Ni_xO_{5+\delta}$ cathodes at $x = 0.2$ and 0.4 are comparable with or slightly higher than that of the $x = 0$ sample,

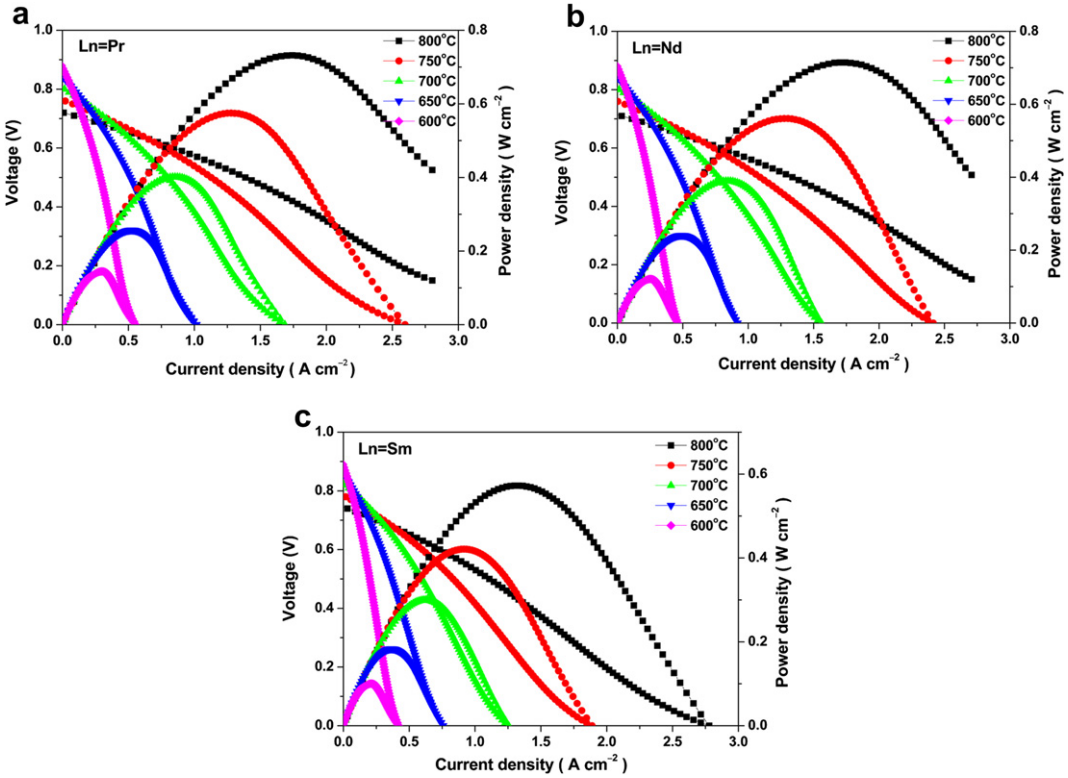

Fig. 7. *I–V* and *I–P* curves of the Ni-SDC/SDC/LnBCN single cells with dry H_2 as the fuel and ambient air as the oxidant in the 600 °C to 800 °C temperature range: (a) PrBCN, (b) NdBCN, and (c) SmBCN.

suggesting that substitution of a small amount of Ni for Co in LnBCN improves the cathode performance. However, the cell performances are lower than those of the $LnBaCo_2O_{5+\delta}$–SDC composite cathodes because of the higher TECs of the LnBCN materials [18]. Improvements in TECs and interfacial properties by the use of LnBCN–SDC composite cathodes require further investigation.

4. Conclusions

$LnBaCo_{1.6}Ni_{0.4}O_{5+\delta}$ (LnBCN, Ln = Pr, Nd, and Sm) materials were prepared and subsequently investigated as potential IT-SOFC cathodes on SDC electrolytes. PrBCN and NdBCN crystallized into a tetragonal structure, while the SmBCN material exhibited an orthorhombic structure. The LnBCN materials are chemically compatible with the SDC electrolyte at temperatures below 950 °C. The substitution of Ni for Co lowered the TEC and ARS of the LnBCN cathodes, thus increasing cell performance. The high electrical conductivity, chemical compatibility, and catalytic activity of the LnBCNs make them good candidates as IT-SOFC cathodes. Although the TECs of LnBCN are lower than those of $LnBaCo_2O_{5+\delta}$ cathodes, these were still higher than those of typical electrolytes. Therefore, further decreases in the TECs of LnBCN materials through the introduction of an ionic conducting phase, such as doped ceria, to form a composite cathode can improve their interfacial and electrochemical performances.

Acknowledgments

This work was supported by the National Fund for Fostering Talents of Basic Science (No. J1103202) and the Innovating Experimentation Project of Jilin University (No. 2010B32031).

References

[1] A. Lashtabeg, S.J. Skinner, Journal of Materials Chemistry 16 (2006) 3161–3170.
[2] S.B. Adler, Chemical Reviews 104 (2004) 4791–4843.
[3] D.J.L. Brett, A. Atkinson, N.P. Brandon, S.J. Skinner, Chemical Society Reviews 37 (2008) 1568–1578.
[4] E.V. Tsipis, V.V. Kharton, Journal of Solid State Electrochemistry 12 (2008) 1367–1391.
[5] T. Hibino, A. Hashimoto, T. Inoue, J. Tokuno, S. Yoshida, M. Sano, Science 288 (2000) 2031–2033.
[6] S.P. Jiang, Journal of Material Science 43 (2008) 6799–6833.
[7] A. Tarancón, M. Burriel, J. Santiso, S.J. Skinner, J.A. Kilner, Journal of Materials Chemistry 20 (2010) 3799–3813.
[8] A.M. Chang, S.J. Skinner, A. Kilner, Solid State Ionics 177 (2006) 2009–2011.
[9] A. Tarancón, A. Morata, G. Dezanneau, S.J. Skinner, J.A. Kilner, S. Estradé, F. Hernández-Ramírez, F. Peiró, J.R. Morante, Journal of Power Sources 174 (2007) 255–263.
[10] G. Kim, S. Wang, A.J. Jacobson, L. Reimus, P. Brodersen, C.A. Mims, Journal of Materials Chemistry 17 (2007) 2500–2505.
[11] A. Tarancón, S.J. Skinner, R.J. Chater, F. Hernández-Ramírez, J.A. Kilner, Journal of Materials Chemistry 17 (2007) 3175–3181.
[12] J.H. Kim, A. Manthiram, Journal of Electrochemical Society 155 (2008) B385–390.
[13] K. Zhang, L. Ge, R. Ran, Z.P. Shao, S.M. Liu, Acta Materialia 56 (2008) 4876–4889.
[14] Q.J. Zhou, T.M. He, Y. Ji, Journal of Power Sources 185 (2008) 754–758.
[15] A. Tarancón, J. Peña-Martínez, D. Marrero-López, A. Morata, J.C. Ruiz-Morales, P. Núñez, Solid State Ionics 179 (2008) 2372–2378.
[16] H. Gu, H. Chen, L. Gao, Y. Zheng, X. Zhu, L. Guo, International Journal of Hydrogen Energy 34 (2009) 2416–2420.
[17] Y. Liu, Journal of Alloys and Compounds 477 (2009) 860–862.
[18] Q.J. Zhou, F. Wang, Y. Shen, T.M. He, Journal of Power Sources 195 (2010) 2174–2181.
[19] A.A. Taskin, A.N. Lavrov, Y. Ando, Applied Physics Letters 86 (2005) 091910.
[20] M.A. Señarís-Rodríguez, J.B. Goodenough, Journal of Solid State Chemistry 118 (1995) 323–336.
[21] K. Huang, H.Y. Lee, J.B. Goodenough, Journal of Electrochemical Society 145 (1998) 3220–3227.
[22] J.H. Kim, A. Manthiram, Electrochimica Acta 54 (2009) 7551–7557.
[23] B. Wei, Z. Lü, D. Jia, X. Huang, Y. Zhang, W. Su, International Journal of Hydrogen Energy 35 (2010) 3775–3782.
[24] A. Bharathi, P. Yasodha, N. Gayathri, A.T. Satya, R. Nagendran, N. Thirumurugan, C.S. Sundar, Y. Hariharan, Physical Review B 77 (2008) 085113.
[25] D. Akahoshi, Y. Ueda, Journal of Solid State Chemistry 156 (2001) 355–363.
[26] A. Maignan, C. Martin, D. Pelloquin, N. Nguyen, B. Raveau, Journal of Solid State Chemistry 142 (1999) 247–260.
[27] I.O. Troyanchuk, N.V. Kasper, D.D. Khalyavin, Physical Review B 58 (1998) 2418–2421.
[28] S.P. Jiang, W. Wang, Journal of Electrochemical Society 152 (2005) A1398–1408.
[29] B.C.H. Steele, Solid State Ionics 86–88 (1996) 1223–1234.
[30] L. Zhao, J.C. Shen, B.B. He, F.L. Chen, C.R. Xia, International Journal of Hydrogen Energy 36 (2011) 3658–3665.
[31] D.J. Chen, R. Ran, K. Zhang, J. Wang, Z.P. Shao, Journal of Power Sources 188 (2009) 96–105.
[32] C.J. Zhu, X.M. Liu, C.S. Yi, L. Pei, D.J. Wang, D.T. Yan, K.G. Yao, T.Q. Lü, W.H. Su, Journal of Power Sources 195 (2010) 3504–3507.
[33] J. Peña-Martínez, A. Tarancón, D. Marrero-López, J.C. Ruiz-Morales, P. Núñez, Fuel Cells 8 (2008) 351–359.
[34] G.Y. Zhu, X.H. Fang, C.R. Xia, X.Q. Liu, Ceramics International 31 (2005) 115–119.
[35] M. Bevilacqua, T. Montini, C. Tavagnacco, E. Fonda, P. Fornasiero, M. Graziani, Chemistry of Materials 19 (2007) 5926–5936.
[36] S. Huang, S. Feng, H. Wang, Y. Li, C. Wang, International Journal of Hydrogen Energy 36 (2011) 10,968–10,974.
[37] N. Ortiz-Vitoriano, I. Ruiz de Larramendi, J.I. Ruiz de Larramendi, M.I. Arriortua, T. Rojo, Journal of Power Sources 196 (2011) 4332–4336.
[38] T. Inoue, T. Setoguchi, K. Eguchi, H. Arai, Solid State Ionics 35 (1989) 285–291.
[39] D. Hirabayashi, A. Tomita, M.E. Brito, T. Hibino, U. Harada, M. Nagao, M. Sano, Solid State Ionics 168 (2004) 23–29.